

## Prompt photons at HERA

*P. J. Bussey*

School of Physics and Astronomy

University of Glasgow

Glasgow, United Kingdom, G12 8QQ

for the ZEUS and H1 Collaborations

### Abstract

The ZEUS detector at HERA has been used to measure the photoproduction of isolated photons in diffractive photoproduction events and deep inelastic scattering (DIS). In the diffractive analysis, cross sections were compared to predictions from the RAPGAP Monte Carlo simulation. First evidence is seen for the direct-photon direct-Pomeron interaction. Cross sections in DIS were evaluated for a number of kinematic two-particle variables and compared to predictions from the AFG and BLZ theoretical models.

### Keywords

HERA; diffraction; photoproduction; deep inelastic scattering; prompt photons; Pomeron

## 1 Experimental method: common features

Results are presented here for the production of isolated hard photons (“prompt” photons) in  $ep$  interactions at HERA. Two analyses are described: one of the diffractive photoproduction of prompt photons, and one of their production in deep inelastic scattering (DIS) processes. The measurements are based on data samples corresponding to integrated luminosities of 82 and 374  $\text{pb}^{-1}$ , taken during the years 1998–2000 and 2004–2007 respectively with the ZEUS detector at HERA, and referred to as HERA-I and HERA-II data respectively. During these periods, HERA ran with an electron or positron beam energy of 27.5 GeV and a proton beam energy of  $E_p = 920$  GeV. The samples include  $e^+p$  and  $e^-p$  data<sup>1</sup>.

Charged particles were measured in the ZEUS central tracking detector and a silicon micro vertex detector, which operated in a solenoidal field of 1.43 T. ZEUS used a uranium-scintillator calorimeter, of which the barrel electromagnetic calorimeter (BEMC) had cells with a pointing geometry aimed at the nominal interaction point. Its fine granularity allowed the use of shower-shape distributions in the measurement of outgoing high-energy photons.

Monte Carlo (MC) event samples were employed to evaluate the detector acceptance and event-reconstruction efficiency, and to provide signal and background distributions. RAPGAP 3.2 [1] was used to generate the diffractive process  $pe \rightarrow pe\gamma X$  for direct and resolved incoming virtual photons at low  $Q^2$ , incident on resolved Pomerons modelled according to the approach of Ingelman and Schlein. The diffractive proton PDF set H1 DPDF Fit B (2006) was used and, for the resolved photon, the PDF set SASGAM 2D. The program PYTHIA 6.416 was used to generate direct and resolved prompt-photon photoproduction processes for background calculations. In the DIS analysis, PYTHIA was used, and also DJANGO interfaced with HERACLES to generate events with initial- and final-state photon radiation from the electron.

The measured photons are accompanied by backgrounds from neutral mesons in hadronic jets, in particular  $\pi^0$  and  $\eta$ , where the meson decay products can create an energy cluster in the BCAL that passes the selection criteria for a photon. In the diffractive analysis these were modelled using RAPGAP

---

<sup>1</sup>Hereafter “electron” refers to both electrons and positrons unless otherwise stated.

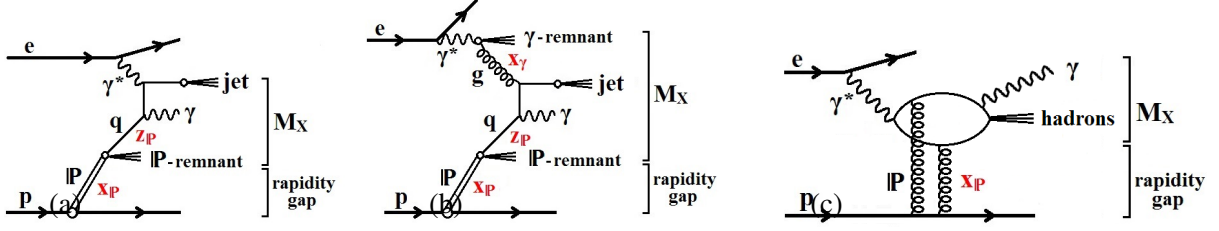


**Fig. 1:** Examples of the diffractive production of a prompt photon and a jet in  $ep$  scattering of a resolved Pomeron from (a) direct (b) resolved photons, and (c) a direct Pomeron process.

events with a dijet final state in which one of the jets resembled a photon candidate. Further diffractive backgrounds came from DIS events and Bethe-Heitler events that produced a photon-electron final state. These were simulated using DJANGO 6 interfaced with HERACLES, and with GRAPE-COMPTON. In the DIS analysis, DJANGO dijet events were used to evaluate the mesonic backgrounds.

The basic event selection and reconstruction were performed as previously [2]. A three-level trigger system was used to select events online. The event analysis made use of energy-flow objects (EFO's), constructed from clusters of calorimeter cells, associated with tracks when appropriate, and also unassociated tracks. Photon candidates were identified as EFO's with no associated track, and with at least 90% of the reconstructed energy measured in the BEMC.

Jets were reconstructed using all the EFO's in the event, including photon candidates, by means of the  $k_T$  clustering algorithm in the  $E$ -scheme in the longitudinally invariant inclusive mode with the radius parameter set to 1.0. To reduce the fragmentation contribution and the background from the decay of neutral mesons within jets, the photon candidate was required to be isolated from other hadronic activity. This was imposed by requiring that the photon-candidate EFO had at least 90% of the total energy of the reconstructed jet of which it formed a part.

Events were selected with the following kinematic conditions. A photon candidate was required with pseudorapidity,  $\eta^\gamma$ , in the range  $-0.7 < \eta^\gamma < 0.9$ . and with reconstructed transverse energy in the range  $5 < E_T^\gamma < 15$  GeV for the diffractive analysis or  $E_T^\gamma > 4$  GeV for the DIS. The hadronic jet, when used, was required to have pseudorapidity,  $\eta^{\text{jet}}$ , range  $-1.5 < \eta^{\text{jet}} < 1.8$ . and transverse energy  $4 < E_T^{\text{jet}} < 35$  GeV for the diffractive analysis or  $E_T^{\text{jet}} > 2.5$  GeV for the DIS. Background events arising from neutral meson decays were subtracted statistically, following the approach taken in previous ZEUS analyses.

It is possible for a photon to be radiated within a jet. Such processes are hard to model within QCD and are suppressed by requiring that the outgoing photon be isolated. Photon isolation was imposed such that at least 90% of the energy of the jet-like object containing the photon originated from the photon.

## 1.1 Kinematic quantities

When a beam proton, with energy  $E_p$ , radiates a Pomeron or equivalent, the fraction of the proton energy taken by the radiated Pomeron is given to a good approximation by the variable  $x_p^{\text{meas}} = (E^{\text{all}} + p_Z^{\text{all}})/2E_p$ , where the suffix ‘‘all’’ refers to all final-state particles or detector-measured objects apart from the forward proton and its possible dissociation products, and excluding the scattered electron. In ‘‘direct’’ photoproduction processes (fig. 1(a)), the entire energy of the incoming photon is absorbed by the target, while in ‘‘resolved’’ processes (fig. 1(b)), the incoming photon's hadronic structure provides a quark or gluon that interacts with a parton from the target. These two classes of process are unambiguously defined only at lowest order, but may be partially distinguished in events containing a high- $E_T$  photon and a jet by means of  $x_\gamma^{\text{meas}} = (E^\gamma + E^{\text{jet}} - p_Z^\gamma - p_Z^{\text{jet}})/(E^{\text{all}} - p_Z^{\text{all}})$ , which measures the fraction of the incoming photon energy that is given to the photon and the jet. The quantities  $E^\gamma$  and  $E^{\text{jet}}$  denote the energies of the photon and the jet, respectively, and  $p_Z$  denotes the corresponding longitudinal

momenta. The presence of direct processes generates a prominent peak in the cross section at high  $x_\gamma^{\text{meas}}$  values. Similarly, direct and resolved Pomeron processes may be defined. The fraction of the Pomeron energy that is taken by the outgoing photon and jet is given to a good approximation by:  $z_{\mathbf{P}}^{\text{meas}} = (E^\gamma + E^{\text{jet}} + p_Z^\gamma + p_Z^{\text{jet}})/(E^{\text{all}} + p_Z^{\text{all}})$ . Figure 1(c) illustrates a possible event type in which the Pomeron is emulated by two exchanged gluons and there is no Pomeron remnant.

## 2 Diffractive analysis

Diffractive hadronic interactions involve the exchange of a colour-neutral object known as the ‘‘Pomeron’’. Diffractive scattering off protons may be initiated by a second incoming hadron, or by a real or virtual photon. At the HERA  $ep$  collider, diffractive processes have been studied both in photoproduction and in deep inelastic scattering, the photoproduction processes consisting of those in which the exchanged virtual photon is quasi-real. The diffractive process is characterized by a forward nucleon, followed by a ‘‘gap’’ in rapidity in which little or no energetic scattering is found until the central region of the process where the hard final state is detected and measured. The present measurements follow an earlier study by H1 [3] of inclusive diffractive high energy prompt photons as a function of transverse momentum. Analyses of isolated photons in non-diffractive photoproduction have also been made by the ZEUS and H1 collaborations [2, 4].

In the measurements presented here, a hard prompt photon is detected in the central region of the ZEUS detector and may be accompanied by a jet [5]. Such processes, while rare, are interesting for several reasons. An outgoing photon must be radiated from a charged partonic object, namely a quark, and therefore demonstrates the presence of a quark content in the Pomeron or of scattering in which both the Pomeron and incident photon couple to quarks. In general, they allow QCD-based models to be tested in order to improve our understanding of a type of process which is important at high energies.

### 2.1 Diffractive selections

To select diffractive events further conditions were applied, the first of which was that the maximum pseudorapidity for EFO’s with energy above 0.4 GeV satisfied  $\eta_{\text{max}} < 2.5$ . A second diffractive condition was that  $x_{\mathbf{P}}^{\text{meas}} < 0.03$ . A selection on the Jacquet–Blondel variable,  $0.2 < y_{\text{JB}} < 0.7$ , removed DIS events. For the HERA-I data sample, the energy in the Forward Plug Calorimeter was required to be less than 1 GeV. This calorimeter was not present in the HERA-II running. A serious background consisted of Bethe-Heitler events containing a high- $E_T$  photon and electron in the final state. These and remaining DIS events were efficiently removed by rejecting events with an identified electron and less than six EFO’s in the detector.

The results are potentially affected by proton-dissociation processes, in which the products of the proton dissociation pass undetected inside the central aperture of the Forward Calorimeter. These were not modelled in the version of RAPGAP that was used. In other ZEUS diffractive analyses, they were estimated to be up to 40% for the HERA-II data and up to 16% for the HERA-I data. The HERA-II data sample was used in the main analysis described here to give the best estimation of the shapes of the cross-section distributions, which were assumed not to depend on the presence of proton dissociation. The HERA-I data were analysed similarly, with the addition of the selection on the additional Forward Plug Calorimeter, and were used to evaluate the total cross section within the selected parameter range. Studies of the event shapes using PYTHIA indicated that the fraction of non-diffractive events in the sample lies between 0% and 10%. This was included in the systematic uncertainties, which were otherwise dominated by the uncertainties in the calorimeter and jet calibration.

### 2.2 Results

Differential cross sections were calculated for the diffractive production of an isolated photon, inclusive and with at least one accompanying jet. The kinematic region was defined by  $Q^2 < 1 \text{ GeV}^2$ ,  $0.2 < y <$

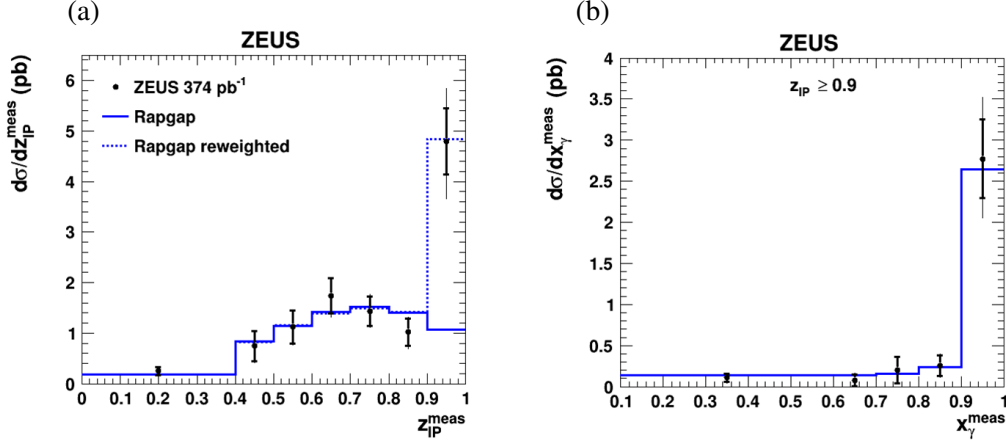


**Fig. 2:** Differential cross sections for events containing an isolated photon accompanied by a jet: (a) as a function of  $z_p^{\text{meas}}$ ; (b) as a function of  $x_\gamma^{\text{meas}}$  for events with  $z_p^{\text{meas}} > 0.9$  at the hadron level. Comparisons are made to normalized predictions from RAPGAP, with and without reweighting. Thick error bars are statistical and thin are statistical combined with systematic.

$0.7, -0.7 < \eta^\gamma < 0.9, 5 < E_T^\gamma < 15$  GeV,  $4 < E_T^{\text{jet}} < 35$  GeV and  $-1.5 < \eta^{\text{jet}} < 1.8$ . The diffractive condition consisted in requirements that  $x_p^{\text{meas}} < 0.03$  and  $\eta^{\text{max}} < 2.5$ . These quantities were evaluated at the hadron level in the laboratory frame, matching the cuts used at the detector level, and the jets were formed according to the  $k_T$  clustering algorithm with the radius parameter set to 1.0.

The results here are inclusive of proton dissociation processes. The total cross section within the observed parameter ranges was found to be  $0.68 \pm 0.14^{+0.06}_{-0.07}$  pb, to be compared to the RAPGAP prediction of 0.68 pb with no proton dissociation and no resolved-suppression factor. It is found that a high fraction of the events with an observed isolated high- $E_T$  photon are accompanied by at least one jet.

Figure 2(a) shows the differential cross section for  $z_p^{\text{meas}}$ , measured using the HERA-II data set. At the upper end of the distribution, a peak is seen which is not described by RAPGAP and which gives evidence for the presence of direct-Pomeron processes. The solid RAPGAP histogram is normalized to the region  $z_p^{\text{meas}} < 0.9$ , while the dashed histogram includes a reweighting factor and is normalized to the entire data distribution. Figure 2(b) shows the  $x_\gamma^{\text{meas}}$  cross section for events with  $z_p^{\text{meas}} > 0.9$  and shows that these events are dominated by a direct-photon component.

Figure 3 shows cross sections for a selection of other variables. The RAPGAP histograms are normalized to the data and describe the shapes of the measured quantities well. Cross sections in  $E_T^{\text{jet}}$  above 15 GeV are omitted from fig. 3(c) owing to limited statistics, but this kinematic region is included in the other cross-section measurements. Figure 3(e) shows the difference in azimuth between the photon and the jet and demonstrates the back-to-back nature of these events. Figure 3(f) shows that the  $x_p^{\text{meas}}$  distribution is well-contained within the selection criterion that was applied.

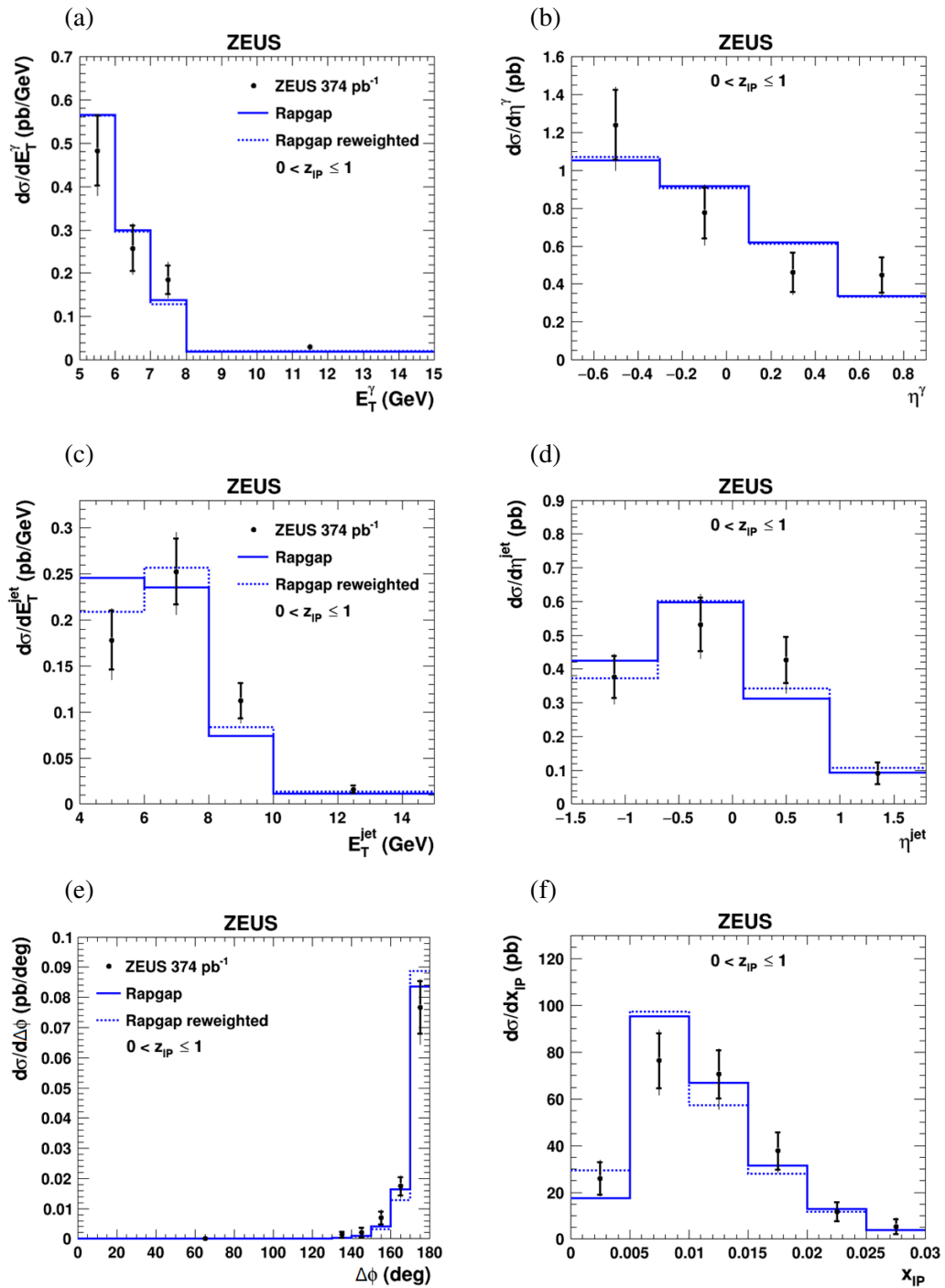


**Fig. 3:** Differential cross sections for events containing an isolated photon accompanied by a jet as functions of: (a)  $E_T^\gamma$ , (b)  $\eta^\gamma$ , (c)  $E_T^{\text{jet}}$ , (d)  $\eta^{\text{jet}}$ , (e)  $\Delta\phi$ , and (f)  $x_{\text{IP}}^{\text{meas}}$ .

### 3 DIS analysis

#### 3.1 Event selections

The DIS analysis used events taken HERA-II only. In each event, a scattered electron was required to be detected with energy above 10 GeV and with polar angle greater than  $140^\circ$  so that the electron was well measured in the ZEUS Rear calorimeter. The value of  $Q^2$  reconstructed from the electron had to be in the range 10–350 GeV<sup>2</sup>.

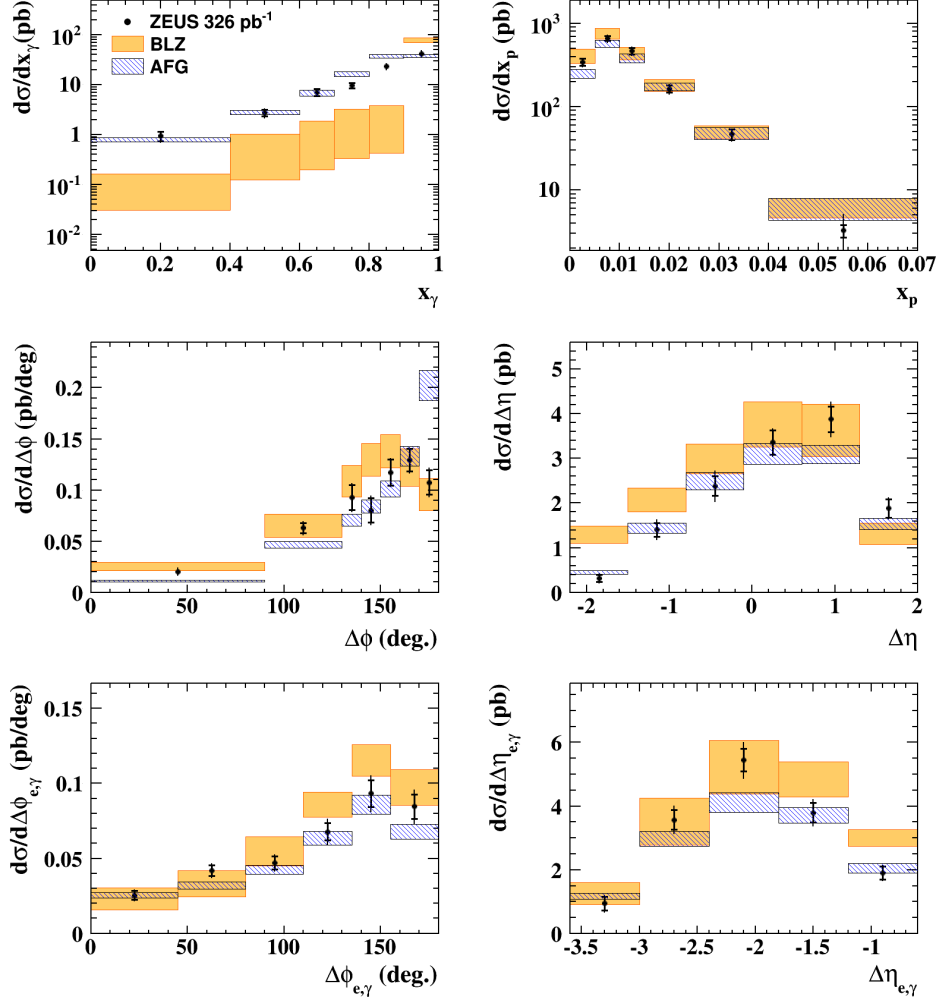


**Fig. 4:** Differential cross sections for DIS events containing an isolated photon accompanied by a jet as functions of:  $x_\gamma^{\text{meas}}$  (top left),  $x_p^{\text{obs}}$  (top right),  $\Delta\phi$  between photon and jet (middle left),  $\Delta\eta$  between photon and jet (middle right),  $\Delta\phi_{e,\gamma}$  (bottom left),  $\Delta\eta_{e,\gamma}$  (bottom right).

#### 3.2 Results

Cross sections for single-particle variables have been published in an earlier paper [6]. The variables presented in Fig. 4 depend on the event as a whole, or on pairs of final-state objects, and are compared to predictions from the theoretical models of AFG [7] and BLZ [8]. These theoretical predictions have corrections applied to them to allow for the conversion of the calculated parton-level final states into the hadronized final states that are corrected. These corrections were calculated using PYTHIA, with no attempt at this stage made to model the PYTHIA to the shape of the calculations at the parton level. Thus, the BLZ prediction displays a delta-function shape in  $x_\gamma^{\text{meas}}$  since no higher-order effects were included.

Further improvements could be made by a reweighting of the PYTHIA in these corrections.

Both models describe the data reasonably well within the theoretical uncertainties, which are based on the QCD scale uncertainty, with the exception of the variable  $x_\gamma^{\text{meas}}$ . For this variable, further correction to the theory would be required to model migration effects downward from the final bin. On the whole, AFG performs slightly better than BLZ.

## References

- [1] H. Jung, <http://www.desy.de/~jung/rapgap.html>
- [2] ZEUS Collaboration, H. Abramowicz *et al.*, Phys. Lett. B 730 (2014) 293
- [3] H1 Collaboration, V. Andreev *et al.*, Phys. Lett. B 672 (2009) 219
- [4] ZEUS Collaboration, J. Breitweg *et al.*, Phys. Lett. B 413 (1997) 201  
 ZEUS Collaboration, J. Breitweg *et al.*, Phys. Lett. B 472 (2000) 175  
 ZEUS Collaboration, S. Chekanov *et al.*, Phys. Lett. B 511 (2001) 19  
 ZEUS Collaboration, S. Chekanov *et al.*, Eur. Phys. J. C 49 (2007) 511  
 H1 Collaboration, A. Aktas *et al.*, Eur. Phys. J. C 38 (2004) 437
- [5] ZEUS Collaboration, H. Abramowicz *et al.*, arXiv:1705.10251
- [6] ZEUS Collaboration, H. Abramowicz *et al.*, Phys. Lett. B 715 (2012) 88
- [7] P. Aurenche, M. Fontannaz and J. Ph. Guillet, , Eur. Phys. J. C 44 (2005) 395
- [8] S. Baranov, A. Lipatov and N. Zotov, Phys. Rev. D81 (2010) 094034